Mechanical & Materials Engineering Faculty Publications

Mechanical & Materials Engineering, Department of

4-1-2023

Plasmon Enhanced Quantum Properties of Single Photon Emitters with Hybrid Hexagonal Boron Nitride Silver Nanocube Systems

Mohammadjavad Dowran

Andrew Butler

Suvechhya Lamichhane

Adam Erickson

Ufuk Kilic

See next page for additional authors

Authors

Mohammadjavad Dowran, Andrew Butler, Suvechhya Lamichhane, Adam Erickson, Ufuk Kilic, Sy_Hwang Liou, Christos Argyropoulos, and A. Laraoui

Plasmon Enhanced Quantum Properties of Single Photon Emitters with Hybrid Hexagonal Boron Nitride Silver Nanocube Systems

Mohammadjavad Dowran, Andrew Butler, Suvechhya Lamichhane, Adam Erickson, Ufuk Kilic, Sy-Hwang Liou, Christos Argyropoulos, and Abdelghani Laraoui*

Hexagonal boron nitride (hBN) has emerged as a promising ultrathin host of single photon emitters (SPEs) with favorable quantum properties at room temperature, making it a highly desirable element for integrated quantum photonic networks. One major challenge of using these SPEs in such applications is their low quantum efficiency. Recent studies have reported an improvement in quantum efficiency by up to two orders of magnitude when integrating an ensemble of emitters such as boron vacancy defects in multilayered hBN flakes embedded within metallic nanocavities. However, these experiments have not been extended to SPEs and are mainly focused on multiphoton effects. Here, the quantum single-photon properties of hybrid nanophotonic structures composed of SPEs created in ultrathin hBN flakes coupled with plasmonic silver nanocubes (SNCs) are studied. The authors demonstrate 200% plasmonic enhancement of the SPE properties, manifested by a strong increase in the SPE fluorescence. Such enhancement is explained by rigorous numerical simulations where the hBN flake is in direct contact with the SNCs that cause the plasmonic effects. The presented strong and fast single photon emission obtained at room temperature with a compact hybrid nanophotonic platform can be very useful to various emerging applications in quantum optical communications and computing.

1. Introduction

Single-photon emitters (SPEs) in solid-state platforms have attracted a large interest over the last decades for various applications in quantum information processing and quantum sensing.[1] Significant developments led to the discovery of a variety of atom-like SPEs in solid-state materials, such as semiconductor quantum dots (e.g., gallium arsenide (GaAs) grown by molecular beam epitaxy)[2] and defect-related color centers in wide bandgap materials, for example, nitrogen vacancy (NV) centers in diamond,[3–8] and divacancies (4H, 6H) in silicon carbide.[9–12] Although substantial recent progress led to understanding and utilizing the quantum properties of SPEs, further advances are severely limited by difficulties in achieving exact placement of quantum emitters, weak light collection due to the high refractive index of bulk substrates, slow emission dynamics, and large-scale integration into photonic nanostructures.[4] Several candidates have been studied as sources for SPEs including tungsten diselenide (WSe_2),[13] molybdenum disulfide (MoS_2),[14] quantum dots,[2] and color centers in wide bandgad semiconductors.[15] Among these sources, hexagonal boron nitride (hBN) has emerged as a promising host of SPEs[16–23] that display promising quantum properties such as narrow emission linewidth at ambient conditions[17] and optically detected magnetic resonance (ODMR),[24] making it a promising material for integrated quantum photonics[1,25,26] and sensing.[27] SPEs have been generated in a large selection of hBN hosts including exfoliated flakes from bulk substrates,[17,18] strain-originated

M. Dowran, A. Erickson, A. Laraoui
Department of Mechanical & Materials Engineerig
University of Nebraska-Lincoln
900 N 16th St. W342 NH, Lincoln, NE 68588, USA
E-mail: alaraoui2@unl.edu

A. Butler, U. Kilic, C. Argyropoulos
Department of Electrical and Computer Engineering
University of Nebraska-Lincoln
844 N. 16th St, Lincoln, NE 68588-1212, USA

S. Lamichhane, S.-H. Liou, A. Laraoui
Department of Physics and Astronomy and the Nebraska Center for Materials and Nanoscience
University of Nebraska-Lincoln
855 N 16th St, Lincoln, NE 68588, USA

C. Argyropoulos
Department of Electrical Engineering
The Pennsylvania State University
203 Electrical Engineering East, University Park, PA 16802, USA

defects in thin hBN flakes,[28] chemical vapor deposition (CVD) grown crystals,[29–31] and commercially available nanoflakes.[32] Various processing techniques have been used to increase the density of SPEs in hBN and improve their quantum properties including annealing at high temperatures (> 850 °C) under Ar and/or O_2 flow,[33] nanoindentation with atomic force microscopy (AFM),[34] plasma treatment,[20] and ion beam implantation of different species (C, O, N).[35] While in most cases, the density of observed SPEs is high (≥ 0.5 emitter in 1 μm^2 area) with narrow emission spectrum, their quantum efficiency is still low with a fluorescence emission rate way below 1 Mc s^{-1}.[33]

Different approaches have been used to increase the fluorescence rates of SPEs in diamond nanocrystals and films by coupling them deterministically with photonics crystals,[36,37] bulls-eye grating,[38,39] and plasmonic nanocavities.[40] However, these methods remain challenging to be applied to hBN due to the difficulty in creating SPEs in hBN nanoflakes[41] with desired spectral properties that match the cavity optical frequency modes. Kim et al. created SPEs on top of hBN photonic crystal by annealing at 850 °C, coupling them spatially within the cavity, and did not see any enhancement in their quantum properties due to the off spectral overlap between the SPEs and the cavity frequency modes.[42] A different approach was used very recently by spreading silver nanocubes (SNCs) on top of hBN flakes containing high-density boron vacancy (V_B^-) emitters deposited on thin metal (Au and Ag) films.[43,44] An overall intensity enhancement of up to 250 times was obtained with a high signal-to-noise ratio (SNR) ODMR signal[43,44] mainly due to the large Purcell enhancement of the plasmonic Ag nanoantennas.[45–47] While those findings are very promising to quantum sensing,[48,49] these experiments were mainly focused on multiphoton effects, such as fluorescence enhancement, and the single photon enhancement from coupling SPEs in hBN flakes with SNCs has not been reported yet.

In this work, we couple SPEs in ultrathin hBN flakes (thickness of 15 nm) to the dominant plasmonic mode of SNCs (size of 98 nm) at room temperature. We experimentally observe a narrowing of the SPEs emission spectra combined with a reduction in their fluorescence lifetime that is accompanied by an enhancement of their single photon fluorescence rate at ambient conditions. Our results provide a first step towards achieving a major speedup and enhancement in the single photon emission of compact nanophotonic devices that can be used in emerging quantum optical applications.[50]

2. Methodology

2.1. Sample Preparation and Creation of SPEs in hBN Flakes

hBN flakes are exfoliated from bulk hBN crystals (hq graphene) using vinyl tape[33] and transferred to a marked 200 nm thick SiO_2/Si substrate. To create a high density (> 0.5 SPE/1 μm^2) of stable SPEs we followed the recipe described in ref. [33] by annealing the hBN flakes on SiO_2/Si substrate under O_2 flow (950 sccm) at a temperature of 1100 °C for 4 h. It is believed that oxygen molecules may break down and react with nitrogen or boron atoms to form different defect species (e.g., oxygen impurities, substitutional oxygen at N or B sites), or take part in the etch-
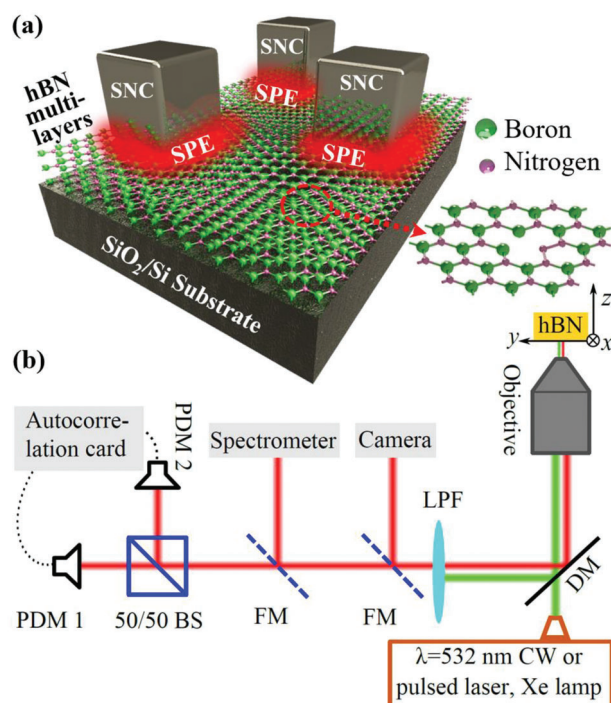
Figure 1. a) Enhanced quantum properties based on hybrid nanophotonic structures composed of SPEs in hBN combined with localized plasmon excitations from SNCs. Insert of a): a sketch of the distribution of hBN flake atoms, composed of boron (green) and nitrogen (purple) atoms in a 2D lattice. b) A schematic of our confocal fluorescence microscope setup consisting of a CCD camera to isolate the hBN flakes, a spectrometer, auto-bunching $g^{(2)}$ setup, lifetime measurements, and fluorescence imaging. DM: dichroic mirror, CW: continuous wave, LPF: long-pass filter, FM: flipped mount mirror, BS: beam splitter.

ing process to form optically active vacancy-related defects.[33,51,52] The hBN flakes were scanned prior to the annealing process to ensure the origin of the defects is not related to the strain variation across the flakes.

We imaged optically different grids on the SiO_2/Si substrate after the annealing process (Section S1, Supporting Information) to identify and select only ultrathin hBN flakes (< 20 nm in thickness). We measured their thickness by using an AFM setup (Section S3, Supporting Information). To enhance the quantum properties of SPEs on a selected thin hBN flake we spin-coated commercial SNCs, with size of 98 ± 7 nm (nanoCopisix), on the annealed SiO_2/Si substrate (**Figure 1**a). We optimized the spin coating parameters to increase the chance of getting the SNCs coupled spatially with the SPEs (Section S5, Supporting Information). We used a home-built confocal fluorescence microscope (Figure 1b) at room temperature to characterize the quantum properties of SPEs in the hBN flakes before and after depositing the SNCs. The setup has four modalities: optical/fluorescence imaging to isolate thin flakes with SPEs, spectroscopy to check the SPE emission wavelength, anti-bunching $g^{(2)}$ experiments to check whether the emitters in hBN are indeed SPEs, and lifetime measurements to measure the SPEs fluorescence lifetime.

ADVANCED
SCIENCE NEWS
www.advancedsciencenews.com

ADVANCED
OPTICAL
MATERIALS
www.advopticalmat.de
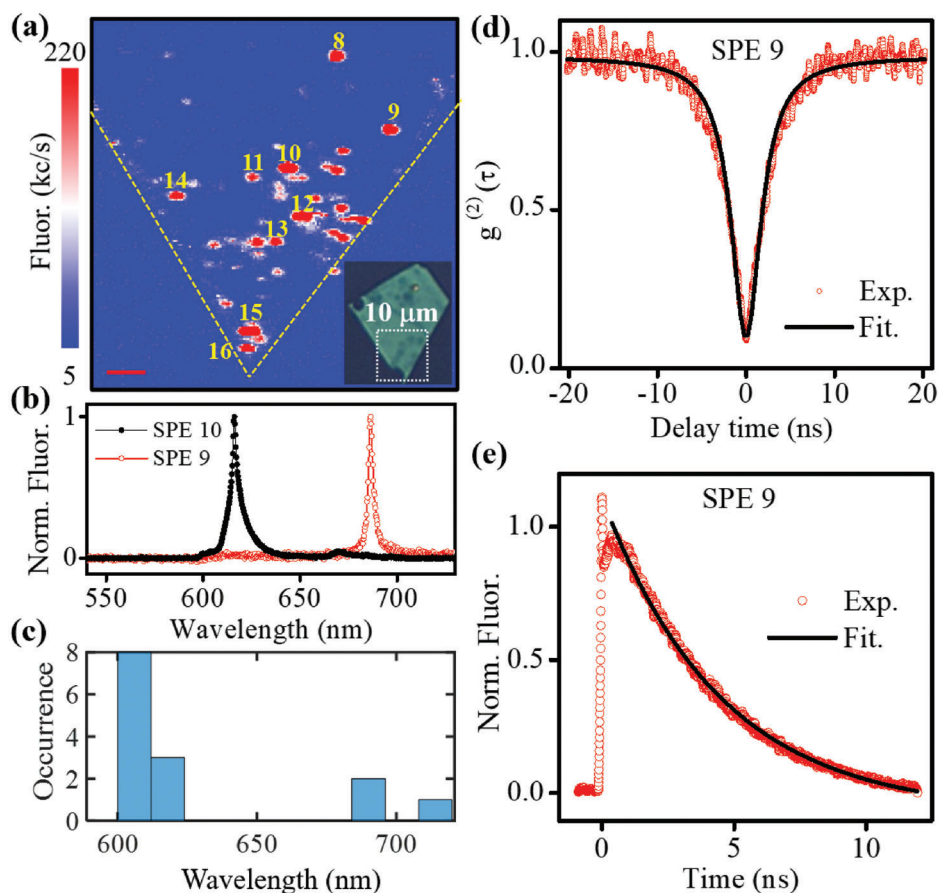
Figure 2. Characterization of the SPEs quantum properties along a selected 15 nm thick hBN flake. a) 10×10 μm fluorescence image of the hBN flake lower part shown in the inset (optical image). Red spots indicate high photon count rates emitted from the flake, where 16 spots were labeled and characterized. b) Spectrum of the fluorescence intensity versus wavelength of two selected emitters SPE 9 and SPE 10 marked in (a). c) Measured emission wavelength distribution of the 16 SPEs characterized in the hBN in (a). d) Autocorrelation $g^{(2)}$ response of emitter SPE 9 as a function of the time delay between the two PDM modules. e) Lifetime response of emitter SPE 9 as a function of time between the 532-nm laser excitation 10 ps pulse and the detected fluorescence in one of the PDM modules. The scale bar in (a) is 1 μm.

2.2. Optical Characterization

To locate the hBN flakes and identify their thickness based on their color[53] a white light (Xe lamp) is focused on the SiO_2/Si substrate and the reflected light is then focused on a CCD camera, as depicted in Figure 1b. We used two types of 532-nm lasers: A CW laser (MLL-FN-532-1000 mW) to perform fluorescence imaging and $g^{(2)}$ measurements, and a 10 ps pulsed laser (SuperK Fianium FIU-15 from NKT Photonics) to measure the fluorescence lifetime. The 532 nm laser is reflected from a dichroic mirror (Semrock, FF560-FDi01) and focused on the hBN flakes using a Nikon oil objective (NA = 1.25). The fluorescence (560–800 nm) emitted from the hBN flake is collected by the same objective, transmitted through the dichroic mirror, and sent to the detection setup to characterize the SPE's quantum properties using flip-mount mirrors. The fluorescence is then focused to a balanced split-single mode fiber (Thorlabs Model TW670R5F1) using 0.25 NA objective and coupled to two single photon detection modules (PDM, Micro Photon Devices). A notch filter (Semrock, NF01-532U-25) is placed in the fluorescence path to block completely the 532-nm excitation light.

The fluorescence imaging of the hBN flake is performed by scanning the SiO_2/Si sample (travel range of 100 μm along x, y, and z) mounted on a closed loop three-axis nanopositioning linear stage (NPXYZ100SG, Newport) and collecting the emitted photons from a confocal spot ($\approx$320 nm) by using one of the PDM modules. **Figure 2**a shows the fluorescence image from the lower corner (10×10 μm) of the hBN flake in the insert of Figure 2a with high density of emitters ($\approx$0.5 μm²). The thickness of the flake is $\approx$15 nm, determined from AFM measurements (Figure S3, Supporting Information). The fluorescence spectrum from each emitter in Figure 2a is recorded by using Solis Triax 320 spectrometer coupled to an Andor camera (iDus 420 CCD). The fluorescence is focused by 75 mm achromatic lens (Thorlabs AC254-075-A) on the spectrometer focal plane and collected through a slit of 50 μm. Figure 2b displays the normalized fluorescence spectra (subtracted from the substrate background) obtained from two selected emitters SPE 9 and SPE 10 in the hBN flake. Sharp emission lines with full width at half-maximum (FWHM) of 2.94 and 6.3 nm are observed by the emitters at 686.5 and 616 nm, respectively. We attribute these peaks to the zero phonon line (ZPL) of the defects.[18] In Figure 2c we plot
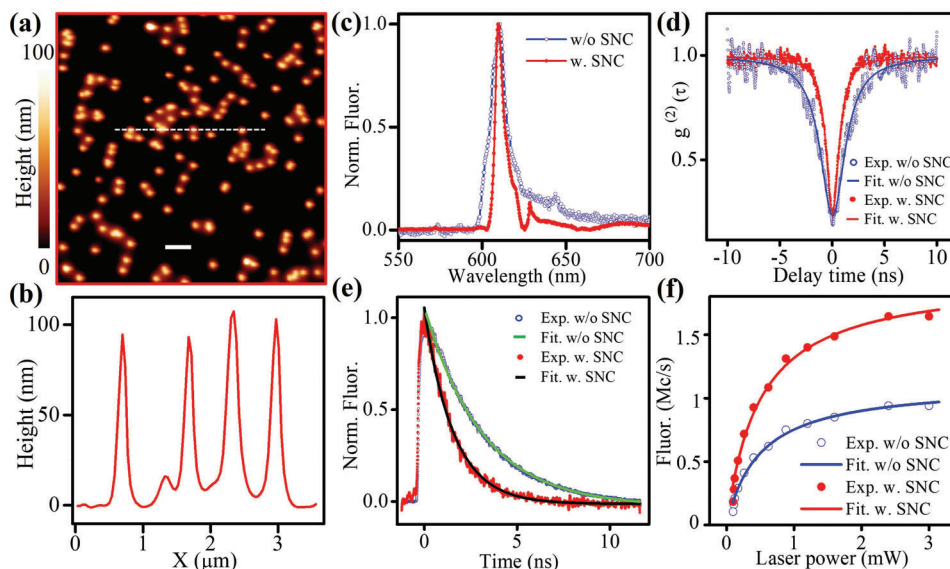
Figure 3. Plasmon-assisted enhancement of SPEs quantum properties. a) A topography map of the SNCs spread on top of the hBN flake in the insert of Figure 2a. b) A transverse cross-cut (scattered line) of the AFM image in (a). The scale bar in (a) is 0.5 μm. The SNCs have a size varying from 95 to 105 nm above the hBN flake (thickness is 15 nm). c) Measured spectra, d) $g^{(2)}$ responses, and e) lifetime rates of SPE 16 before (open-circle scattered) and after (filled-circle scattered) depositing the 98 nm Ag cube. f) Measured (scattered) and calculated (solid lines) fluorescence intensity of SPE 16 versus CW green laser power before (open-circle scattered) and after (filled-circle scattered) depositing the 98 nm Ag cube. The red and blue lines in (f) are fitted curves according to ref. [58].

the histogram of the ZPL peaks occurrence as a function of wavelength for 16 SPEs (see Table S1, Supporting Information) from the hBN flake in Figure 2a and found that all emitters are centered in a spectral window of 600–710 nm with a negligible phonon side band (PSB). This correlates well with recent studies done on SPEs created by annealing hBN flakes under O_2 flow.[33]

To check the single-photon emission properties of the emitters in Figure 2a, we performed anti-bunching $g^{(2)}$ measurements in the Hanbury Brown and Twiss (HBT) configuration. We used a time-tagger device (PicoHarp 300) to measure the autocorrelation $g^{(2)}$ response from the photons collected by the two PDM modules as a function of time delay t between the two detectors (±20 ns). We found > 90% of the emitters in Figure 2a have a dip of $g^{(2)}$ < 0.25 (Figure 2d, and Table S1, Supporting Information), a clear indication of SPEs.[47] For short time scales ($t \lesssim 20$ ns), the $g^{(2)}$ response of the SPEs (e.g., emitter 9 in Figure 2d) is normalized and fitted to the following equation: $g^{(2)}(t) \simeq 1 - (1 + a_1)e^{-t/\tau_1}$, where a_1 is the anti-bunching factor and τ_1 is the excited state lifetime which includes both the radiative and nonradiative transition lifetimes.[54,55] We obtain $a = -0.47 \pm 0.05$ and $\tau_1 = 2.9$ ns ± 0.15 ns by fitting the measured curve in Figure 2d (solid line).

To measure the excited-state lifetime of the emitters, we used a 10 ps pulsed green laser to excite the emitters and a time-tagger device (PicoHarp 300) to perform time-dependent photon statistics. For this experiment, the time tagger measures the time difference between the excitation 10 ps pulse and the detected SPE photons of the PDM detector. We calibrated the lifetime setup and found a response function (IRF) of 19 ps. The lifetime signal is normalized and found to be fitted with only one exponential model using the following equation: $a_2 e^{-t/\tau_3}$, where t is the varying time, τ_3 is the fluorescence lifetime, and a_3 is the weighing factor.[18] The lifetime τ_3 of SPE 9 is ≈4.5 ± 0.23 ns (**Figure 3**e)

and it varies from 1 to 5 ns for the 16 SPEs studied in the hBN flake in Figure 2a (see Table S1, Supporting Information).

3. Results and Discussion

3.1. Plasmon Enhancement of the SPEs Quantum Properties in a Hybrid hBN-SNC System

We measured the SPE optical properties before and after spin-coating of 98 ± 7 nm SNCs on top of the hBN flake depicted in the insert of Figure 2a. By using an overlay method, and by verifying the spectra of the emitting spots, we identified the location of the labeled SPEs after spin coating of the SNCs. We detail the distribution of the spin-coated SNCs on top of the hBN flake in Figure S4, Supporting Information. We verified the distribution of the SNCs on the hBN flake by AFM analysis of the SNCs (Figure 3a) and confirmed the size of the cubes of 98 ± 7 nm (Figure 3b). Moreover, the plasmonic spectral mode of the silver nanocube supports only a selection of emission modes from the SPEs in the hBN flake in the spectral region around the nanocube's resonance frequency. Hence, not all emission modes from SPEs get enhanced and, therefore, the wavelength response of SPEs gets narrower, as was demonstrated before in the photoluminescence spectrum of a relevant nanocube cavity system combined with MoS_2.[56] This effect is also present in our system and depicted in Figure 3c with a decrease in the FWHM of the ZPL peak by 30%. We demonstrate a plasmonic enhancement of the quantum properties of emitter SPE 16 manifested by a narrowing of the $g^{(2)}$ response (Figure 3d) and a decrease in the fluorescence lifetime from 3.13 ± 0.16 to 1.56 ± 0.08 ns (Figure 3e). The plasmon SPE enhancement rate $\frac{\frac{1}{\tau_{w.SNC}}}{\frac{1}{\tau_{w/oSNC}}} = \frac{\tau_{w/oSNC}}{\tau_{w.SNC}} = 2$ corresponds to

**ADVANCED
SCIENCE NEWS**

www.advancedsciencenews.com

**ADVANCED
OPTICAL
MATERIALS**

www.advopticalmat.de
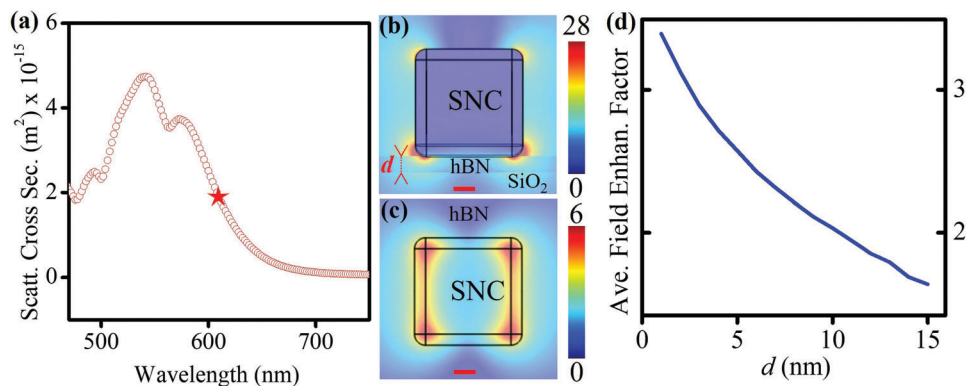
Figure 4. Simulation results of the hybrid hBN-SNC system plasmonic modes. a) Computed scattering cross-section spectrum that shows a higher-order resonance near 550 nm. b) Side and c) top views of the field enhancement factor along a 98 nm SNC demonstrating the electric field distribution of the plasmonic resonance mode at wavelength 610 nm corresponding to the wavelength of SPE 16 studied in Figure 3. d) The average electric field enhancement factor as a function of the distance d in hBN, as sketched in (b). The scale bar in (b,c) is 20 nm.

an enhancement rate of 200%. We attribute this to both the Purcell effect that leads to a radiative rate enhancement and the lossy nature of the plasmonic SNC structure which increases the non-radiative rate. Both effects are related to the local confinement of the electric field at the SNC surface,[45,46,57] confirmed by COMSOL modeling (see discussion below). The excited state lifetime reduction is dominated by the increase in the efficiency of the defect radiative decay, confirmed by measuring the decay rate enhancement with the saturated intensity enhancement (below).[58] The enhancement factor varies across SPEs. For example, in SPE 9 there is no enhancement and in SPE 15 we observe an enhancement factor of 70% (Figure S6, Supporting Information). We explain this variation by the non-spatial (e.g., SPE 10) and/or non-spectral (e.g., SPE 9) overlap between the SPE and the SNC localized plasmon modes in the range of 450–650 nm computed and presented in **Figure 4**a.

To know the saturated count rate of the emitter before and after spin coating the SNCs (size of 98 nm) we measured the fluorescence intensity of SPE 16 as function of the CW laser power and found a saturation count rate of ≈1 Mc s^{-1} without SNC (open circle line in Figure 3f) and a saturation count rate of ≈2 Mc s^{-1} with SNC (filled-circle line in Figure 3f). The saturation curves for the SPE 16 with and without SNC are fitted (Figure 3f) to:[58] $I = \frac{I_\infty P}{(Psat+P)}$, where I_∞ is the saturated count rate and P_{Sat} is the saturation power. $I_{\infty, w/o\ SNC} = 0.97$ Mc s^{-1} and $I_{\infty, w.\ SNC} = 1.7$ Mc s^{-1} for the uncoupled and coupled SPE respectively. The enhancement factor $\frac{I_{\infty,w.SNC}}{I_{\infty,w/oSNC}}$ is 1.75, which is dominated by the enhancement of the radiative decay channel.[58] The saturation power curve of the coupled SPE-SNC system is subtracted from the fluorescence emission power dependence of an isolated SNC away from the emitter on the hBN flakes (Figure S5, Supporting Information). Therefore, the saturation curve for the SPE 16 with SNC is assumed to originate solely from the plasmonic-enhanced fluorescence of the SPE. The difficulty in measuring the SPE saturation count rate after depositing the nanocubes arises from the high-intensity autofluorescence generated by the 98 nm SNCs in the 600–700 nm spectral window (up to 5 Mc s^{-1} at saturation, Figure S5, Supporting Information). However, an increase in the SNR of the SPE 16 with SNC fluorescence is clearly depicted in

Figure 3c,d where the measurements are taken at the same averaging time before and after spin coating the SNCs.

3.2. Modeling the Plasmonic Modes of the SNC-hBN System

The finite-element method simulation software (COMSOL Multiphysics) was used to accurately model the scattering response of the SNCs. The SNC was encased in a spherical domain with scattering boundary conditions to mimic an open boundary. The edges of the Ag nanocube were 98 nm long and smoothed with a radius of 10 nm curvature to be closer to the shape of the experimental samples. All the appropriate substrate materials below the nanocube were included in our calculations. The hBN, Ag, SiO$_2$, and Si materials that compose the currently studied system were all modeled using their frequency-dependent dielectric constants.[59–62] To calculate the scattering cross section, the scattered-field formulation was used which considers the analytical solution for an incident plane wave in the absence of the nanocube as the background electric field. The incident plane wave is transverse-magnetic (TM) polarized and impinges upon the cube under normal incidence. The scattering energy is calculated by measuring the power of the field scattered by the cube. This energy is then divided by the geometrical cross-section of the SNC to compute the scattering cross-section. Since the nanocube structure is symmetric, identical scattering results are obtained when the incident plane wave is transverse-electric (TE) polarized or incoherently polarized containing both TE and TM polarizations. Figure 4a shows part of the scattering cross-section as a function of the wavelength. A broad scattering plasmon resonance is observed in the range 450–650 nm at the central wavelength of 550 nm. We plot the electric field enhancement factor at a wavelength of 610 nm from the 98-nm SNC in Figure 4b (side view) and Figure 4c (top view) and demonstrate an increase of 28 times at the edges of the Ag cube. Since the SPE location across the hBN thickness cannot be determined experimentally by optical measurements, we integrated the overall field enhancement as a function of the distance d from the Ag cube across the hBN multilayer. We observe an overall field enhancement of 3 (300%) at the interface of hBN and Ag cube reduced to 1.6 (60%)

along the interface of hBN and SiO$_2$ with results demonstrated in Figure 4d. The extent of the field enhancement from an SNC is related to the evanescent waves of the plasmonic excitations localized on the surface of the SNC, and decays as the measurement plane gets farther away from the SNC, as depicted in Figure 4d. This correlates well with the enhancement factor of the fluorescence lifetime and intensity measured on SPE 16 (Figure 3) and SPE 15 (Figure S6, Supporting Information).

4. Conclusion

In summary, we demonstrated the coupling of silver nanocube plasmonic modes (98 nm in size) with SPEs in layered 15 nm thick hBN flakes. An overall enhancement of the SPE fluorescence lifetime and intensity of up to 200% is obtained, corresponding to a saturation count rate > 2 Mc s^{-1}. We confirmed the measured plasmonic enhancement of the SPE properties by using finite-element method simulations to accurately model the scattering response of the hybrid SNC-SPE system. The presented strong and fast single photon emission obtained at room temperature with a hybrid nanophotonic platform can be very useful to various emerging applications in quantum optical communications and computing. To better improve the spatial and spectral overlap of the SPEs in hBN with the optical frequencies of the metal nanocavities a combination of processing and nanofabrication methods must be followed. This includes a deterministic creation of SPEs in hBN flakes deposited on epitaxial metal films (high reflectivity) by for example nanoindentation with AFM,[34] followed by precise nanofabrication of dielectric or metal nanostructures such as photonics crystals,[36] bullseye grating,[38,39] and plasmonic nanocavities.[40] However, even the current results prove that room-temperature solid-state quantum emitters in hBN or other 2D van der Waals (vdW) materials[63] can be an ideal platform for integrated quantum photonics.[1,25,26]

Supporting Information

Supporting Information is available from the Wiley Online Library or from the author.

Conflict of Interest

The authors declare no conflict of interest.

Author Contributions

M.D. synthesized the hBN flakes, performed the optical measurements, and analyzed the data; A.B. performed COMSOL modeling; S.L. and S.-H.L. prepared the SiO$_2$/Si substrates and made the marks; A.E. assisted M.D. in the AFM measurements; U.K. helped in the designs in Figure 1 and performed ellipsometry measurements (not reported here) to check the optical properties of SiO$_2$/Si substrates. A.L. and C.A. designed the experiments and supervised the project. A.L. wrote the manuscript with the contributions of all authors. All authors have given approval to the final version of the manuscript.

Data Availability Statement

The data that support the findings of this study are available from the corresponding author upon reasonable request.

[1] I. Aharonovich, D. Englund, M. Toth, *Nat. Photonics* **2016**, *10*, 631.
[2] P. Senellart, G. Solomon, A. White, *Nat. Nanotechnol.* **2017**, *12*, 1026.
[3] V. Acosta, Hemmer, *MRS Bull.* **2013**, *38*, 127.
[4] M. Atatüre, D. Englund, N. Vamivakas, S.-Y. Lee, J. Wrachtrup, *Nat. Rev. Mater.* **2018**, *3*, 38.
[5] A. Laraoui, J. S. Hodges, C. A. Meriles, *Nano Lett.* **2012**, *12*, 3477.
[6] M. E. Trusheim, L. Li, A. Laraoui, E. H. Chen, H. Bakhru, T. Schröder, O. Gaathon, C. A. Meriles, D. Englund, *Nano Lett.* **2014**, *14*, 32.
[7] A. Laraoui, K. Ambal, *Appl. Phys. Lett.* **2022**, *121*, 060502.
[8] A. Erickson, S. Q. A. Shah, A. Mahmood, I. Fescenko, R. Timalsina, C. Binek, A. Laraoui, *RSC Adv.* **2023**, *13*, 178.
[9] B. Diler, S. J. Whiteley, C. P. Anderson, G. Wolfowicz, M. E. Wesson, E. S. Bielejec, F. Joseph Heremans, D. D. Awschalom, *npj Quantum Inf.* **2020**, *6*, 1.
[10] D. J. Christle, A. L. Falk, P. Andrich, P. V. Klimov, J. U. Hassan, N. T. Son, E. Janzén, T. Ohshima, D. D. Awschalom, *Nat. Mater.* **2015**, *14*, 160.
[11] J.-F. Wang, Q. Li, F.-F. Yan, H. Liu, G.-P. Guo, W.-P. Zhang, X. Zhou, L.-P. Guo, Z.-H. Lin, J.-M. Cui, X.-Y. Xu, J.-S. Xu, C.-F. Li, G.-C. Guo, *ACS Photonics* **2019**, *6*, 1736.
[12] W. F. Koehl, B. B. Buckley, F. J. Heremans, G. Calusine, D. D. Awschalom, *Nature* **2011**, *479*, 84.
[13] K. Parto, S. I. Azzam, K. Banerjee, G. Moody, *Nat. Commun.* **2021**, *12*, 3585.
[14] J. Klein, M. Lorke, M. Florian, F. Sigger, L. Sigl, S. Rey, J. Wierzbowski, J. Cerne, K. Müller, E. Mitterreiter, P. Zimmermann, T. Taniguchi, K. Watanabe, U. Wurstbauer, M. Kaniber, M. Knap, R. Schmidt, J. J. Finley, A. W. Holleitner, *Nat. Commun.* **2019**, *10*, 2755.
[15] M. D. Eisaman, J. Fan, A. Migdall, S. V. Polyakov, *Rev. Sci. Instrum.* **2011**, *82*, 071101.
[16] I. Aharonovich, J.-P. Tetienne, M. Toth, *Nano Lett.* **2022**, *22*, 9227.
[17] T. T. Tran, C. Zachreson, A. M. Berhane, K. Bray, R. G. Sandstrom, L. H. Li, T. Taniguchi, K. Watanabe, I. Aharonovich, M. Toth, *Phys. Rev. Appl.* **2016**, *5*, 034005.
[18] T. T. Tran, K. Bray, M. J. Ford, M. Toth, I. Aharonovich, *Nat. Nanotechnol.* **2016**, *11*, 37.
[19] T. T. Tran, C. Elbadawi, D. Totonjian, C. J. Lobo, G. Grosso, H. Moon, D. R. Englund, M. J. Ford, I. Aharonovich, M. Toth, *ACS Nano* **2016**, *10*, 7331.

**ADVANCED
SCIENCE NEWS**

www.advancedsciencenews.com

**ADVANCED
OPTICAL
MATERIALS**

www.advopticalmat.de

[20] Z.-Q. Xu, C. Elbadawi, T. T. Tran, M. Kianinia, X. Li, D. Liu, T. B. Hoffman, M. Nguyen, S. Kim, J. H. Edgar, X. Wu, L. Song, S. Ali, M. Ford, M. Toth, *Nanoscale* **2018**, *10*, 7957.

[21] C. Li, Z.-Q. Xu, N. Mendelson, M. Kianinia, M. Toth, I. Aharonovich, *Nanophotonics* **2019**, *8*, 2049.

[22] T. Gao, M. von Helversen, C. Antón-Solanas, C. Schneider, T. Heindel, *npj 2D Mater. Appl.* **2023**, *7*, 1.

[23] C. Zhang, Z. Shi, T. Wu, X. Xie, *Adv. Opt. Mater.* **2022**, *10*, 2200207.

[24] H. L. Stern, Q. Gu, J. Jarman, S. Eizagirre Barker, N. Mendelson, D. Chugh, S. Schott, H. H. Tan, H. Sirringhaus, I. Aharonovich, M. Atatüre, *Nat. Commun.* **2022**, *13*, 618.

[25] J. D. Caldwell, I. Aharonovich, G. Cassabois, J. H. Edgar, B. Gil, D. N. Basov, *Nat. Rev. Mater.* **2019**, *4*, 552.

[26] M. Toth, I. Aharonovich, *Annu. Rev. Phys. Chem.* **2019**, *70*, 123.

[27] C. L. Degen, F. Reinhard, P. Cappellaro, *Rev. Mod. Phys.* **2017**, *89*, 035002.

[28] G. Grosso, H. Moon, B. Lienhard, S. Ali, D. K. Efetov, M. M. Furchi, P. Jarillo-Herrero, M. J. Ford, I. Aharonovich, D. Englund, *Nat. Commun.* **2017**, *8*, 705.

[29] N. Nikolay, N. Mendelson, E. Özelci, B. Sontheimer, F. Böhm, G. Kewes, M. Toth, I. Aharonovich, O. Benson, *Optica* **2019**, *6*, 1084.

[30] N. Mendelson, Z.-Q. Xu, T. T. Tran, M. Kianinia, J. Scott, C. Bradac, I. Aharonovich, M. Toth, *ACS Nano* **2019**, *13*, 3132.

[31] H. Liu, C. Y. You, J. Li, P. R. Galligan, J. You, Z. Liu, Y. Cai, Z. Luo, *Nano Mater. Sci.* **2021**, *3*, 291.

[32] M. K. Boll, I. P. Radko, A. Huck, U. L. Andersen, *Opt. Express* **2020**, *28*, 7475.

[33] Y. Chen, C. Li, S. White, M. Nonahal, Z.-Q. Xu, K. Watanabe, T. Taniguchi, M. Toth, T. T. Tran, I. Aharonovich, *ACS Appl. Mater. Interfaces* **2021**, *13*, 47283.

[34] X. Xu, Z. O. Martin, D. Sychev, A. S. Lagutchev, Y. P. Chen, T. Taniguchi, K. Watanabe, V. M. Shalaev, A. Boltasseva, *Nano Lett.* **2021**, *21*, 8182.

[35] N. Mendelson, D. Chugh, J. R. Reimers, T. S. Cheng, A. Gottscholl, H. Long, C. J. Mellor, A. Zettl, V. Dyakonov, P. H. Beton, S. V. Novikov, C. Jagadish, H. H. Tan, M. J. Ford, M. Toth, C. Bradac, *Nat. Mater.* **2021**, *20*, 321.

[36] D. Englund, B. Shields, K. Rivoire, F. Hatami, J. Vučković, H. Park, M. D. Lukin, *Nano Lett.* **2010**, *10*, 3922.

[37] A. Faraon, C. Santori, Z. Huang, V. M. Acosta, R. G. Beausoleil, *Phys. Rev. Lett.* **2012**, *109*, 033604.

[38] L. Li, E. H. Chen, J. Zheng, S. L. Mouradian, F. Dolde, T. Schröder, S. Karaveli, M. L. Markham, D. J. Twitchen, D. Englund, *Nano Lett.* **2015**, *15*, 1493.

[39] G. Yang, Q. Shen, Y. Niu, H. Wei, B. Bai, M. H. Mikkelsen, H. Sun, *Laser Photonics Rev.* **2020**, *14*, 1900213.

[40] S. I. Bogdanov, M. Y. Shalaginov, A. S. Lagutchev, C.-C. Chiang, D. Shah, A. S. Baburin, I. A. Ryzhikov, I. A. Rodionov, A. V. Kildishev, A. Boltasseva, V. M. Shalaev, *Nano Lett.* **2018**, *18*, 4837.

[41] J. A. Preuß, E. Rudi, J. Kern, R. Schmidt, R. Bratschitsch, *2D Mater.* **2021**, *8*, 035005.

[42] S. Kim, J. E. Fröch, J. Christian, M. Straw, J. Bishop, D. Totonjian, K. Watanabe, T. Taniguchi, M. Toth, *Nat. Commun.* **2018**, *9*, 2623.

[43] N. Mendelson, R. Ritika, M. Kianinia, J. Scott, S. Kim, J. E. Fröch, C. Gazzana, M. Westerhausen, L. Xiao, S. S. Mohajerani, S. Strauf, M. Toth, I. Aharonovich, Z. Xu, *Adv. Mater.* **2022**, *34*, 2106046.

[44] X. Xu, A. B. Solanki, D. Sychev, X. Gao, S. Peana, A. S. Baburin, K. Pagadala, Z. O. Martin, S. N. Chowdhury, Y. P. Chen, T. Taniguchi, K. Watanabe, I. A. Rodionov, A. V. Kildishev, T. Li, P. Upadhyaya, A. Boltasseva, V. M. Shalaev, *Nano Lett.* **2022**, *23*, 25.

[45] T. B. Hoang, G. M. Akselrod, C. Argyropoulos, J. Huang, D. R. Smith, M. H. Mikkelsen, *Nat. Commun.* **2015**, *6*, 7788.

[46] G. M. Akselrod, C. Argyropoulos, T. B. Hoang, C. Ciracì, C. Fang, J. Huang, D. R. Smith, M. H. Mikkelsen, *Nat. Photonics* **2014**, *8*, 835.

[47] O. Iff, Q. Buchinger, M. Moczała-Dusanowska, M. Kamp, S. Betzold, M. Davanco, K. Srinivasan, S. Tongay, C. Antón-Solanas, S. Höfling, C. Schneider, *Nano Lett.* **2021**, *21*, 4715.

[48] A. J. Healey, S. C. Scholten, T. Yang, J. A. Scott, G. J. Abrahams, I. O. Robertson, X. F. Hou, Y. F. Guo, S. Rahman, Y. Lu, M. Kianinia, I. Aharonovich, J.-P. Tetienne, *Nat. Phys.* **2023**, *19*, 87.

[49] M. Huang, J. Zhou, D. Chen, H. Lu, N. J. McLaughlin, S. Li, M. Alghamdi, D. Djugba, J. Shi, H. Wang, C. R. Du, *Nat. Commun.* **2022**, *13*, 5369.

[50] S. I. Bogdanov, A. Boltasseva, V. M. Shalaev, *Science* **2019**, *364*, 532.

[51] P. Ares, H. Santos, S. Lazić, C. Gibaja, I. Torres, S. Pinilla, J. Gómez-Herrero, H. P. Meulen, P. García-González, F. Zamora, *Adv. Electron. Mater.* **2021**, *7*, 2001177.

[52] L. Weston, D. Wickramaratne, M. Mackoit, A. Alkauskas, *Phys. Rev. B* **2018**, *97*, 214104.

[53] Y. Anzai, M. Yamamoto, S. Genchi, K. Watanabe, T. Taniguchi, S. Ichikawa, Y. Fujiwara, H. Tanaka, *Appl. Phys. Express* **2019**, *12*, 055007.

[54] S. C. Kitson, P. Jonsson, J. G. Rarity, P. R. Tapster, *Phys. Rev. A* **1998**, *58*, 620.

[55] E. Wu, V. Jacques, H. Zeng, P. Grangier, F. Treussart, J.-F. Roch, *Opt. Express* **2006**, *14*, 1296.

[56] G. M. Akselrod, T. Ming, C. Argyropoulos, T. B. Hoang, Y. Lin, X. Ling, D. R. Smith, J. Kong, M. H. Mikkelsen, *Nano Lett.* **2015**, *15*, 3578.

[57] C. Ciracì, A. Rose, C. Argyropoulos, D. R. Smith, *J. Opt. Soc. Am. B* **2014**, *31*, 2601.

[58] M. Nguyen, S. Kim, T. T. Tran, Z.-Q. Xu, M. Kianinia, M. Toth, *Nanoscale* **2018**, *10*, 2267.

[59] Y. Rah, Y. Jin, S. Kim, K. Yu, *Opt. Lett.* **2019**, *44*, 3797.

[60] P. B. Johnson, R. W. Christy, *Phys. Rev. B* **1972**, *6*, 4370.

[61] L. V. Rodríguez-de Marcos, J. I. Larruquert, J. A. Méndez, J. A. Aznárez, *Opt. Mater. Express* **2016**, *6*, 3622.

[62] C. Schinke, P. Christian Peest, J. Schmidt, R. Brendel, K. Bothe, M. R. Vogt, I. Kröger, S. Winter, A. Schirmacher, S. Lim, H. T. Nguyen, D. MacDonald, *AIP Adv.* **2015**, *5*, 067168.

[63] S. Ren, Q. Tan, J. Zhang, *J. Semicond.* **2019**, *40*, 071903.